Springer

Acta Mechanica Sinica

CrossMark click for updates

• Research Paper •

Acta Mech. Sin., Vol. 42, 225780 (2026)
https://doi.org/10.1007/s10409-025-25780-x

Influence of water-soaking on the mechanical properties of liquid crystal elastomers: an experimental study

Wenhui Chen[1], Xiaohang Zhou[1], Junmou Tang[2], Ruobing Bai[3], Liu Wang[4,5], and Ke Liu[1*]

[1] *School of Advanced Manufacturing and Robotics, Peking University, Beijing 100871, China;*
[2] *Department of Bioengineering, Imperial College London, London SW7 2AZ, UK;*
[3] *Department of Mechanical and Industrial Engineering, College of Engineering, Northeastern University, Boston MA 02115, USA;*
[4] *Department of Modern Mechanics, School of Engineering Science, University of Science and Technology of China, Hefei 230027, China;*
[5] *The State Key Laboratory of Nonlinear Mechanics, Beijing 100090, China*

Received November 10, 2025; accepted November 25, 2025

Abstract: Liquid crystal elastomers (LCEs) are increasingly used as artificial muscles to power a variety of soft robots. Although LCEs exhibit similar deformation upon stimulation in both air and water, experiments reveal that their mechanical properties are significantly compromised after soaking in water, which prohibits long-term underwater usage. In this work, we systematically investigate how and why water affects the mechanical properties of LCEs, considering two commonly used liquid crystal monomers: C6M and C3M. Through soaking and dehydration experiments combined with mechanical testing, molecular dynamics simulations, and Fourier-transform infrared spectroscopy, we reveal that water induces both swelling and chemical degradation that result in notably reduced mechanical strength. Furthermore, we try different strategies to prevent such strength reduction, including tuning oxygen content, varying crosslink density, and eliminating oxygen-containing crosslinkers, but achieve limited success, as swelling and chemical degradation persist. Despite these unsuccessful attempts, we demonstrate that encapsulating LCEs with a butyl rubber-based coating presents an effective waterproofing strategy, significantly preventing the mechanical strength reduction. This study provides a fundamental understanding of the mechanical properties of soaked LCEs and thus provides practical guidelines for developing durable LCE-powered robots for underwater environments.

Keywords: Soft materials, Underwater robot, Liquid crystal elastomer (LCE), Soft actuator, Soft robot

Citation: W. Chen, X. Zhou, J. Tang, R. Bai, L. Wang, and K. Liu, Influence of water-soaking on the mechanical properties of liquid crystal elastomers: an experimental study, Acta Mech. Sin. **42**, 225780 (2026), https://doi.org/10.1007/s10409-025-25780-x

1. Introduction

Liquid crystal elastomers (LCEs) are stimuli-responsive smart materials capable of reversible, muscle-like actuation under thermal, optical, or electrical stimulation [1-9]. Their ability to undergo large, programmable deformations makes them ideal candidates for constructing soft actuators and shape-morphing systems in the fields of soft robotics and biomedical devices [10-16]. As these devices increasingly operate in challenging and humid environments, such as in-body or underwater conditions, the interaction between LCEs and aquatic environments has become a subject of growing importance [17-23].

Previous studies on LCE-water interactions have focused on two aspects: (1) water-driven LCEs, where researchers investigate diverse deformation modes triggered by water stimuli (e.g., swelling, dissolution) [24-27]; (2) submerged LCE actuators, designed to operate in aquatic environments, with emphasis on their actuation efficiency for underwater soft robotics [20, 28-30]. While both scenarios demand robust mechanical output and long-term durability for reliable performance, systematic investigations into LCE behavior in water remain limited [31-34]. In particular, factors such

*Corresponding author. E-mail address: liuke@pku.edu.cn (Ke Liu)

as water absorption [35-37], hydrolytic degradation [38, 39], or the plasticizing effect [40, 41] of water may significantly influence the mechanical properties and longevity of LCE-based actuators. Yet, how these factors evolve over time remains poorly understood. This knowledge gap continues to hinder the development of robust and long-lasting LCE-based soft robots for underwater applications, underscoring the need for investigations into LCE-water interactions [2, 42-45].

In this work, we address this critical question through a systematic study of LCE mechanical behavior under water soaking (Fig. 1). Specifically, we investigate how water influences LCE mechanical performance, such as whether swelling or internal damage dominates the decrease of modulus, and what strategies can preserve LCE functionality in water. By resolving these fundamental mechanisms, our study provides essential insights for designing durable LCE actuators capable of reliable operation in underwater and biomedical applications.

This paper is structured as follows. Section 2 describes the preparation of LCE samples, divided into two subsections detailing the synthesis protocols for C6M-based and C3M-based LCEs. Section 3 investigates the mechanical performance of oriented LCEs before soaking, after soaking, and following dehydration, revealing significant loss in strength and modulus: swelling causes reversible softening (partially recovered after dehydration), whereas chemical degradation results in irreversible damage. Section 4 extends the study to non-oriented LCEs, which also exhibit mechanical loss dominated more by reversible swelling and less by irreversible chemical degradation. Section 5 explores strategies to mitigate water-induced property loss, including tuning oxygen content, adjusting crosslink density, and removing oxygen-containing crosslinkers. However, these approaches cannot fully prevent degradation. In contrast, applying a waterproof coating effectively blocks water ingress, preserving both mechanical properties and actuation performance. Finally, Sect. 6 summarizes key findings and provides design guidelines for durable, underwater-stable LCE actuators and soft robots.

2. Preparation of LCE samples

To ensure the generalizability and relevance of our findings, we prepare two types of thermally actuated LCEs using widely adopted liquid crystal monomers, C6M (a flexible monoacrylate mesogen, a.k.a. RM82) and C3M (a rigid diacrylate mesogen, a.k.a. RM257). These two formulations differ significantly in their nematic-to-isotropic transition temperature (T_{NI}) (Fig. A1 in Appendix A), crosslink density, and mechanical behaviors, making them representative for exploring the effects of aquatic environments across a range of LCE chemistries.

2.1 Preparation of the C6M-based LCE

The C6M-based LCE is made by mixing 1,4-bis-[4-(6-acryloyloxyhexyloxy)benzoyloxy]-2-methylbenzene (1, C6M, Macklin, 98%), poly(ethylene glycol) diacrylate (2, PEG400, Macklin reagent), 1,2-Bis(2-mercaptoethoxy)ethane (3,6-Dioxa-1,8-octanedithiol) (3, EDDET, Sigma-Aldrich, 95%), pentaerythritol tetrakis(3-mercapto-propionate) (4, PETMP, Aladdin Biochemical, 98%), butylated hydroxytoluene (BHT) (5, BioRuler, 98%), 2,2-Dimethoxy-2-phenylacetophenone (6, 651), triethylamine (7, TEA, Concord Technology, 99%) (Fig. 2(a)).

For the preparation, we combined C6M (0.8520 g, 1.27 mmol), BHT (0.0216 g, 0.098 mmol), PEG400 (0.1476 g, 0.37 mmol), EDDET (0.3180 g, 1.74 mmol), TEA (0.0099 g, 0.098 mmol), 651 (0.0072 g, 0.028 mmol), and PETMP (0.1485 g, 0.30 mmol) in a vial and melted the mixture. After thorough stirring and degassing, the sample is placed in a 100 °C oven for 8 h, followed by ultraviolet (UV) light curing for 90 min to complete the polymerization process.

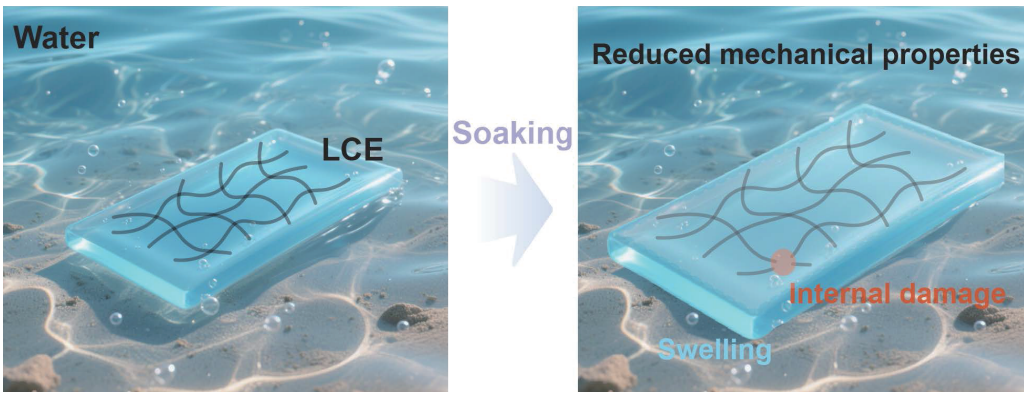

Figure 1 Schematic illustration of the change of LCEs after water-soaking.

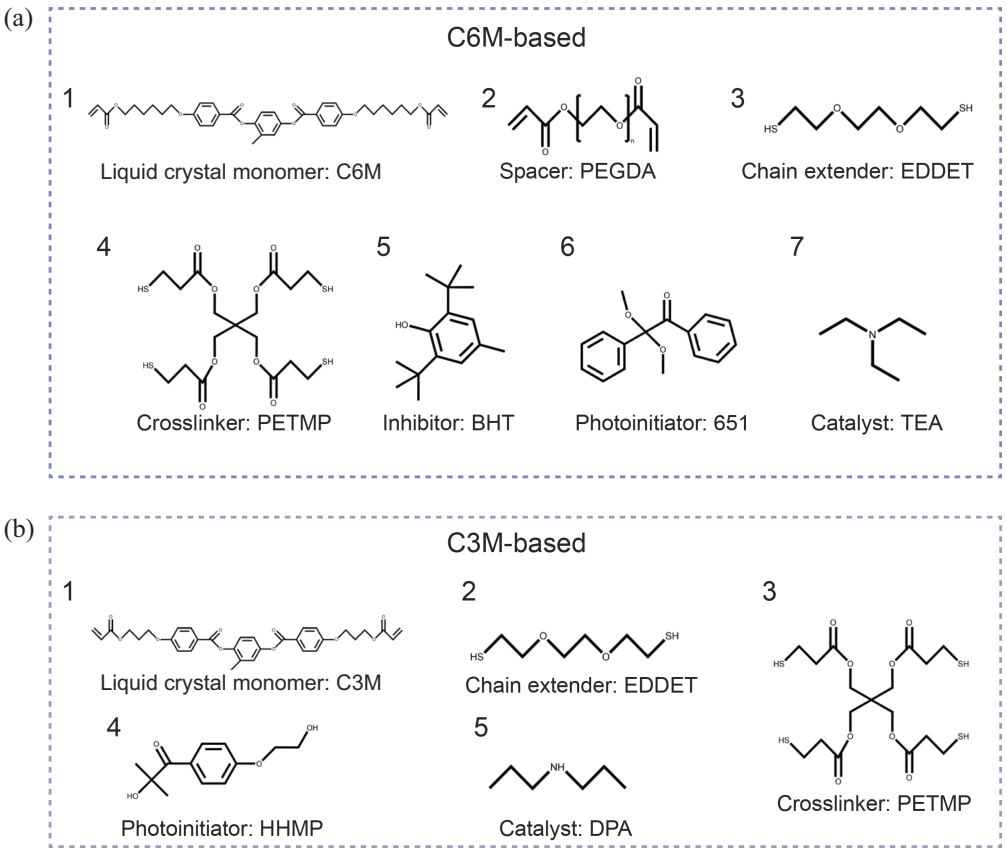

Figure 2 Schematic of the formulation of two kinds of LCE: (a) C6M-based LCE formula and (b) C3M-based LCE formula.

2.2 Preparation of the C3M-based LCE

The C3M-based LCE is made by mixing 1,4-Bis-[4-(3 - acryloyloxypropyloxy) benzoyloxy] - 2 - methylbenzene (1, C3M, HwrkChemical Technology, 98%), 1,2-Bis(2-mercaptoethoxy)ethane (3,6-Dioxa-1,8-octanedithiol) (2, EDDET, Sigma-Aldrich, 95%), pentaerythritol tetrakis(3-mercapto-propionate) (4, PETMP, Aladdin Biochemical, 98%), BHT (5, BioRuler, 98%), 2-Hydroxy-4-(2-hydroxyethoxy)-2-methylpropiophenone (4, HHMP, Aladdin Biochemical, 98%), dipropylamine (5, DPA, Aladdin Biochemical, 99%), and toluene (Tong Guang Fine Chemicals, 99.5%) (Fig. 2(b)).

For the C3M-based LCE synthesis, we combined C3M (0.5460 g, 0.93 mmol), HHMP (0.0035 g, 0.016 mmol), EDDET (0.1250 g, 0.29 mmol), PETMP (0.0296 g, 0.061 mmol), and DPA (0.0015 g, 0.015 mmol) with toluene (0.2490 g, 2.70 mmol) in a vial and melted the mixture. After thorough stirring and degassing, we transferred the solution into a rectangular mold and allowed it to stand at room temperature for 24 h. The sample is then placed in a 100 °C oven for an additional 24 h to ensure complete solvent evaporation, followed by UV light curing for 3 min to complete the polymerization process.

3. Mechanical performance of oriented LCEs under water-soaking

We first investigate the mechanical behavior of oriented LCEs under water-soaking. We soak both C6M-based and C3M-based LCEs in deionized water at 25 °C for various durations: 1, 2, 3, 4, 5, 6, and 7 days, as well as until saturation is reached. At each soaking duration, a portion of the samples is removed, weighed, and then dehydrated until their weight returns to the original dry value. This procedure provides paired samples in both soaked and dehydrated states at each soaking duration, enabling direct comparison of water-induced effects on mechanical performance.

Over time, water absorption, measured as percentage weight gain, increases consistently, with oxygen-rich C6M-based LCEs absorbing more water than C3M-based LCEs (Fig. 3(a) and (b)). Meanwhile, optical transparency decreases proportionally with soaking duration. This effect is more pronounced in C6M-based LCEs (Fig. 3(c)). Taken together, these changes in mass and optical clarity indicate that water does not merely adhere to the surface, but permeates deeply into the LCE material (Fig. 3(e)).

To further evaluate the impact of water absorption on the mechanical behavior of oriented LCEs, we perform tensile

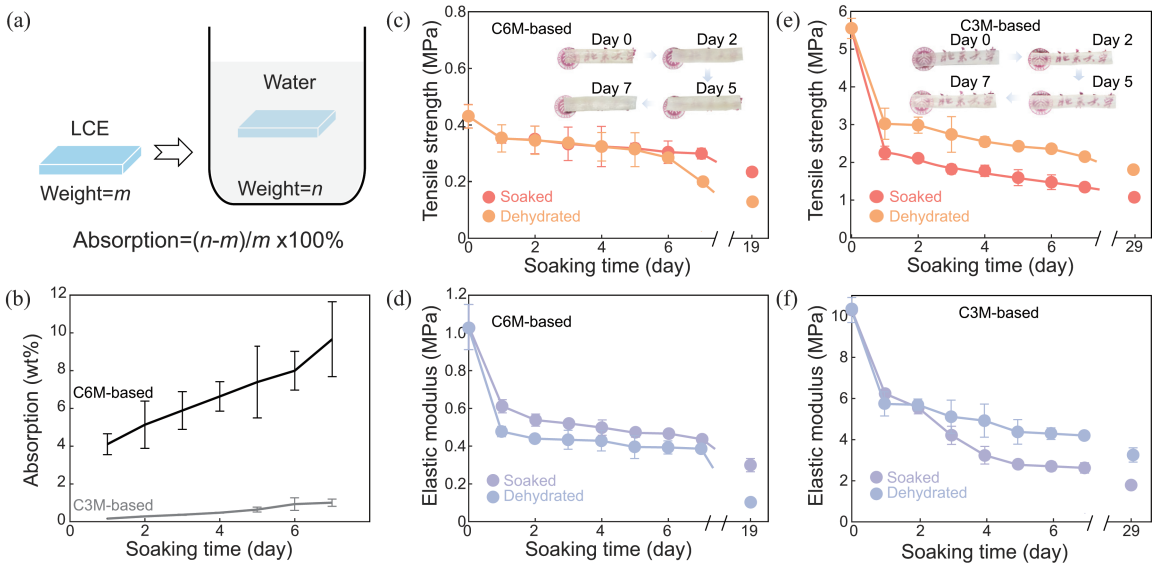

Figure 3 Effect of water-soaking on the mechanical properties of oriented LCEs. (a) Illustration of the calculation of water absorption. (b) Water absorption of LCEs as a function of soaking duration. (c) Tensile strength of soaked and dehydrated C6M-based LCEs with different soaking durations (insets: photographs of soaked samples). (d) Elastic moduli of soaked and dehydrated C6M-based LCEs with different soaking durations. (e) Tensile strength of soaked and dehydrated C3M-based LCEs with different soaking durations (insets: photographs of soaked samples). (f) Elastic moduli of soaked and dehydrated C3M-based LCEs with different soaking durations.

tests on both soaked and dehydrated samples (Fig. 3(c)–(f)) using a universal mechanical testing system (Series F, Mark-10) equipped with a 50 N load cell. The results reveal that the mechanical performance of soaked oriented LCEs, specifically their tensile strength and modulus, decreases after water-soaking. The reduced mechanical performance becomes more pronounced with longer soaking duration, corresponding to higher water absorption. The C3M-based LCE, which absorbs less water, exhibits a more significant reduction in mechanical properties compared to the more highly soaked C6M-based LCE. This counterintuitive result may be attributed to the more uniform water penetration in the C6M-based LCE, which could help preserve its structural integrity to some extent.

In addition, we examined whether the water-induced reduction in mechanical properties could be reversed after dehydration. We found that the mechanical performance of LCEs only partially recovered, reaching less than 50% of the original value (Fig. 3(c)–(f)). This limited recovery suggests that the reduction is not solely due to reversible swelling, but is predominantly caused by irreversible internal damage from water infiltration, highlighting the vulnerability of oriented LCEs to long-term water exposure.

To substantiate this hypothesis and explore the underlying molecular mechanisms, we further conducted molecular dynamics (MD) simulations and performed Fourier-transform infrared (FTIR) spectroscopy (Bruker Vertex 70). These complementary approaches allow us to characterize both the swelling behavior and possible chemical or structural changes contributing to irreversible damage.

In the MD simulations, we use the large-scale atomic/molecular massively parallel simulator (LAMMPS23) [46, 47] with the all-atom optimized potentials for liquid simulations (OPLS-AA) force field [48] to model atomic interactions. The initial molecular structures are built using the PACKMOL software [49, 50], followed by energy minimization via the steepest descent algorithm [51].

To reproduce the crosslinked polymer network at the molecular scale, we adopted a two-step construction procedure. First, a pre-equilibrated mixture containing precursor monomers and crosslinkers was generated. Then, a crosslinking simulation was performed using a custom Python script based on the PySIMM package, which algorithmically formed covalent bonds when reactive sites approached within a predefined cutoff distance. This process effectively mimicked experimental curing until the target crosslinking density was reached. The resulting network was further minimized and equilibrated to obtain a structurally stable configuration.

Building upon this equilibrated structure, different swelling states were modeled by immersing the crosslinked network into a solvent-saturated simulation box. The swelling ratio was controlled by adjusting the box dimensions to represent specific levels of solvent uptake. The system was equilibrated under the NpT ensemble (298 K, 101 kPa) until both the polymer-solvent interface and overall density reached equilibrium, thereby replicating experimen-

tally observed swelling behavior.

To explore how molecular alignment influences water-polymer interactions, both oriented and non-oriented LCE configurations were constructed. The oriented state was generated by arranging mesogenic units into a pre-organized crystalline structure with highly aligned directors, while the non-oriented state was obtained by heating the ordered melt to a high temperature, followed by rapid quenching, freezing a disordered configuration. The degree of alignment was quantified by the global orientational order parameter (S), defined as the largest eigenvalue of the order parameter tensor calculated from mesogen orientation vectors. The two systems exhibited distinct mesoscopic organization, with $S > 0.6$ for the oriented state and $S < 0.2$ for the non-oriented state.

Finally, all systems were equilibrated under the NpT ensemble (T = 298 K, p = 101 kPa) using a Nose-Hoover thermostat, followed by a 100 ps equilibration with a timestep of 0.1 fs. Production runs were then carried out under the NVT ensemble for 200 ps. Simulation trajectories were visualized and analyzed using OVITO [52].

Based on the equilibrated MD trajectories, we evaluate how water absorption influences the mechanical properties of oriented LCEs. As these simulations exclusively capture the swelling process without accounting for internal damage, the observed deterioration in tensile strength, elastic modulus, and elongation at break (Fig. 4(c)–(e)) can be attributed directly to swelling effects (Fig. 4(a) and (b)). This finding

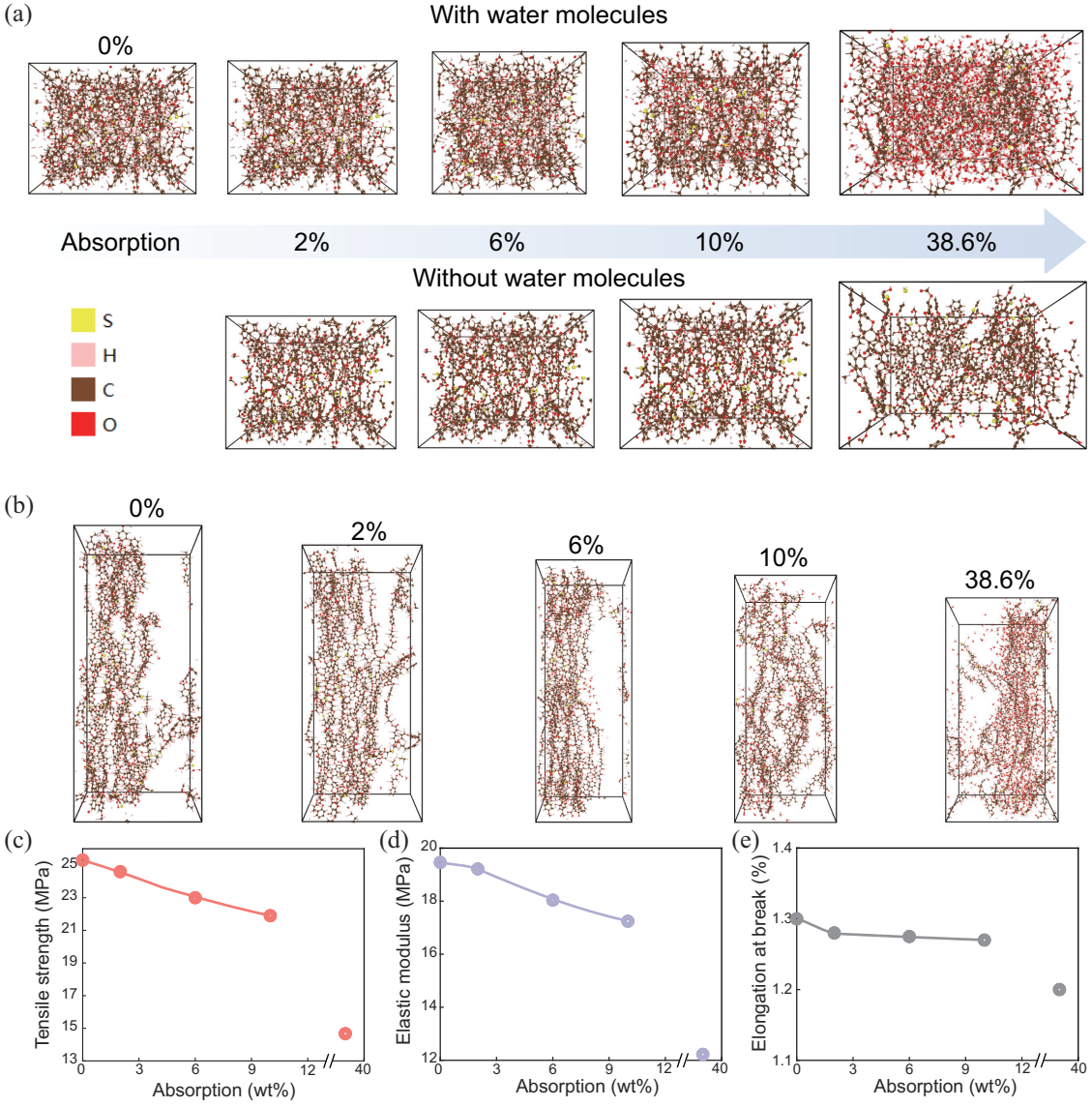

Figure 4 Molecular dynamics simulation of the swelling process of C3M-based LCE at 25 °C. (a) Molecular configurations of LCE with and without absorbed water molecules. (b) 3D representations of soaked LCEs at different levels of water absorption. (c) Tensile strength, (d) elastic modulus, and (e) elongation at break of soaked LCEs.

demonstrates that swelling alone imposes a detrimental effect on mechanical performance.

While the MD simulations reveal that swelling alone negatively affects mechanical performance, they do not capture possible chemical degradation processes that might further weaken the polymer network. To explore potential chemical degradation mechanisms beyond physical swelling, we conduct FTIR spectroscopy on both C6M-based and C3M-based LCEs after water soaking and subsequent dehydration (Fig. 5(a) and (b)). After a cycle of soaking and dehydration, we find that both types of LCEs exhibit weakened ether bond signals after soaking, suggesting that water-soaking chemically degrades oxygen-containing bonds within the polymer network. As shown in Fig. 5, the intensities of the C=C stretching band (1620 cm^{-1}) and the C=O stretching band (1720 cm^{-1}) gradually decrease with immersion time. After one day of soaking, the normalized intensity of the C=O band decreased by approximately 2% for the C6M-based LCE and 1% for the C3M-based LCE, while the C=C band decreased by about 30% and 27%, respectively. These quantitative spectral changes confirm the partial cleavage of ester linkages and side-chain degradation, leading to irreversible chemical damage in the polymer network and, consequently, a further reduction in mechanical properties.

In summary, our results demonstrate that water-soaking reduces the mechanical properties of oriented LCEs through the combined effects of physical swelling and chemical degradation. The negative impact intensifies with increasing water absorption: swelling disrupts mesogen alignment and softens the polymer network, while FTIR analysis reveals that hydrolysis of labile ether bonds plays a dominant role in the deterioration process. Overall, irreversible internal damage caused by chemical bond cleavage emerges as the primary driver of the reduction in mechanical properties under aquatic conditions.

4. Mechanical performance of non-oriented LCEs under water-soaking

Having examined the water-induced mechanisms of the reduction in mechanical properties of oriented LCEs, we next turn to investigate the mechanical performance of non-oriented LCEs under aquatic conditions. In practical applications, LCE actuators contract upon thermal stimulation as they transition into an isotropic and disordered state. Therefore, understanding their mechanical properties in this thermally activated and non-oriented condition is particularly relevant for water-interactive environments. To explore this, we introduce temperature gradients in the soaking water, covering conditions below and above the T_{NI}. This design enables us to assess how thermal activation, in combination with water-soaking, affects the structural integrity and mechanical performance of LCEs across different phase states.

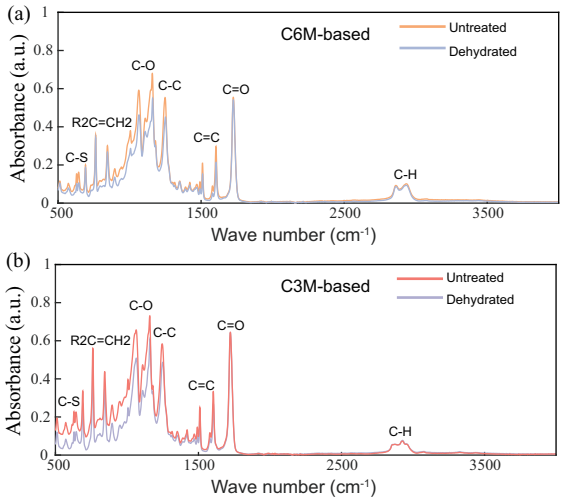

Figure 5 FTIR spectra of (a) C6M-based and (b) C3M-based LCEs before (untreated) and after dehydration (dehydrated). Characteristic absorption peaks corresponding to different functional groups are used to analyze structural changes upon dehydration.

To quantify how thermal activation affects water interaction, we measured the water absorption of C6M-based LCEs at different temperatures spanning below and above the T_{NI}. As shown in Fig. 6, the water absorption of C6M-based LCEs increases with temperature, indicating an enhanced water uptake capacity at elevated temperatures. However, once the temperature exceeds the T_{NI}, the rate of water absorption slows significantly. This behavior may be attributed to the loss of the non-oriented phase.

In addition to measuring water absorption, we also evaluated the thermally induced actuation strain of C6M-based LCEs under different soaking conditions to determine whether water uptake affects their deformation behavior. Interestingly, despite temperature-dependent increases in water absorption, the thermally induced deformation of the LCEs remains largely unaffected (Figs. 6(b) and 7(b)). This suggests a potential decoupling between actuation strain and water absorption. Such a phenomenon may partly explain why previous studies have paid limited attention to the mechanical degradation of underwater LCEs: although water infiltration occurs, the macroscopic actuation behavior appears largely preserved.

Building on the observed temperature-dependent water absorption and stable actuation strain, we next evaluated the tensile strength of C6M-based LCEs in their non-oriented state across the temperature range. As temperature increases, tensile strength declines markedly, mirroring the trend in water uptake. Moreover, samples subjected to dehydration after soaking do not fully recover their original mechanical prop-

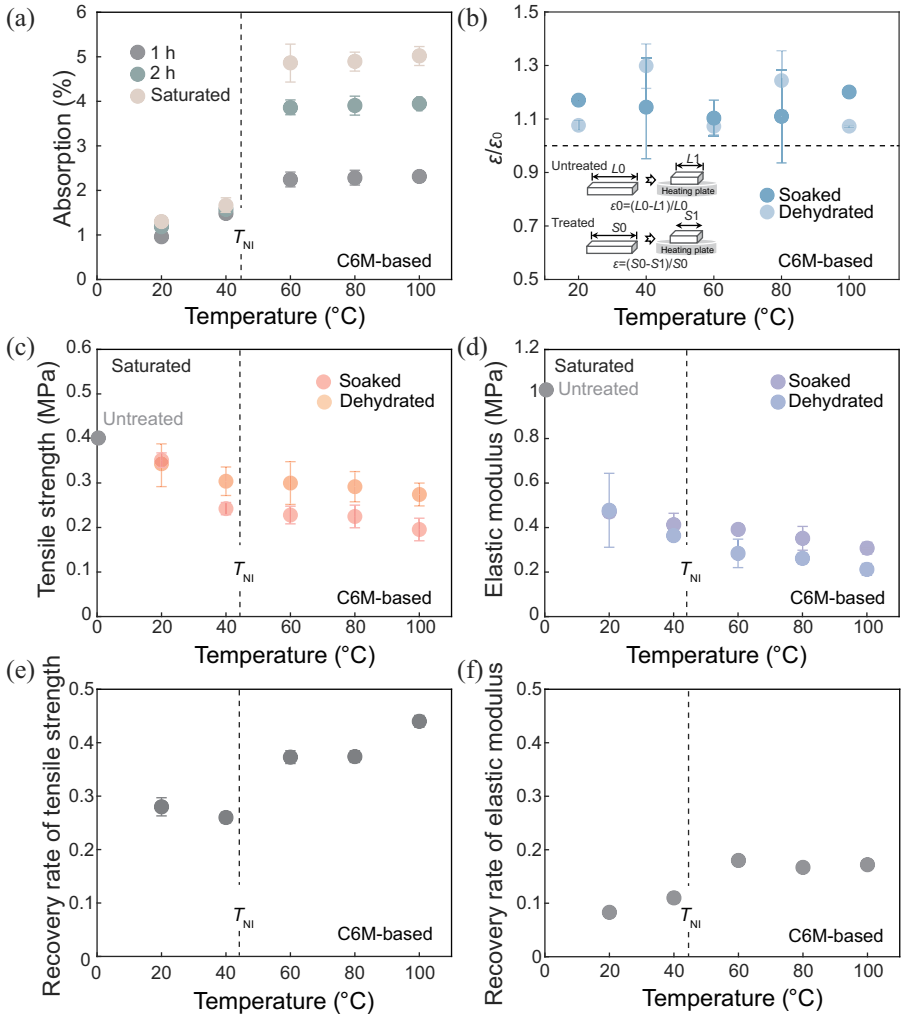

Figure 6 Underwater performance of C6M-based LCEs under different soaking temperatures. (a) Water absorption of C6M-based LCEs under different soaking temperatures. (b) Actuation strain ratio of C6M-based LCEs under different soaking temperatures. The insets show the definition of the actuation strain ratio. (c) Tensile strength and the (d) elastic moduli of the C6M-based LCEs under different soaking temperatures. The recovery rate of (e) tensile strength and (f) elastic modulus of C6M-based LCEs under different soaking temperatures. The data for oriented samples are represented by the data points to the left of the vertical dashed line (indicating T_{NI}), while the data for non-oriented samples are shown to the right.

erties, indicating irreversible internal damage. These results suggest that, similar to the oriented state, the mechanical degradation in non-oriented LCEs arises from a combined effect of swelling and permanent structural damage, with the latter playing a dominant role.

To better understand the factors governing the reduction in mechanical properties of LCEs, we quantify the recovery rate of tensile strength and elastic modulus following dehydration, defined as the ratio of post-dehydration to initial values. We find that non-oriented C6M-based LCEs consistently exhibit higher recovery rates compared to oriented ones. This difference likely reflects the structural anisotropy inherent to oriented LCEs, where water-induced disruption of mesogen alignment results in more severe and largely irreversible damage. Conversely, the absence of long-range molecular order in non-oriented LCEs reduces alignment-related damage, making swelling-induced effects relatively more prominent in their mechanical decline. Nevertheless, internal damage remains the dominant factor compromising mechanical performance in both states. These observations hold consistently across the tested temperature range (Fig. 6(e) and (f)), providing valuable insight into the distinct mechanisms in oriented versus non-oriented LCEs.

Similar trends were observed in C3M-based LCEs, reinforcing the generality of the mechanisms discussed above. As shown in Fig. 7(e) and (f), samples based on C3M exhibit comparable water absorption behavior and reduction of mechanical properties under equivalent thermal and hydration conditions. The temperature-dependent increase in water uptake and the partial recovery after dehydration closely mirror those seen in the C6M-based systems. This consistency indicates that the thermally modulated interaction between wa-

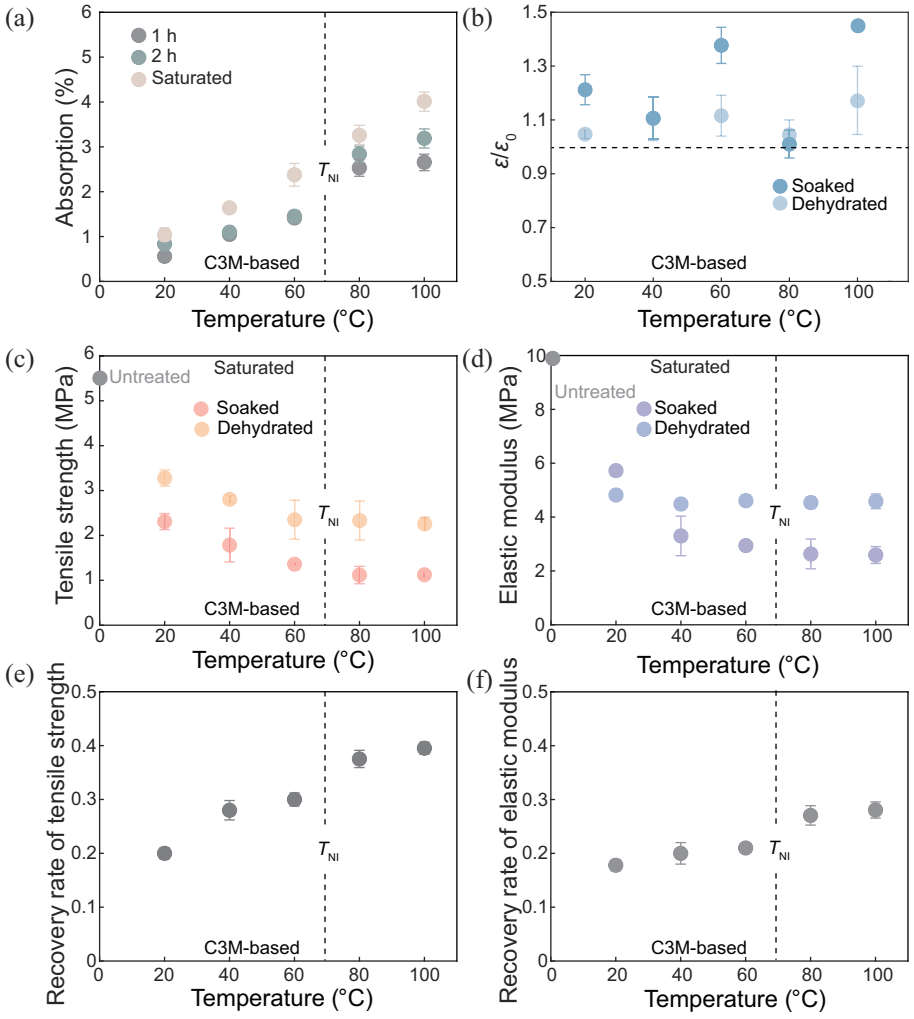

Figure 7 Underwater performance of C3M-based LCEs under different soaking temperatures. (a) Water absorption of C3M-based LCEs under different soaking temperatures. (b) Actuation strain ratio of C3M-based LCEs under different soaking temperatures. The insets show the definition of the actuation strain ratio. (c) Tensile strength and the (d) elastic modulus of the C3M-based LCEs under different soaking temperatures. The recovery rate of (e) tensile strength and (f) elastic modulus of C3M-based LCEs under different soaking temperatures. The data for oriented samples are represented by the data points to the left of the vertical dashed line (indicating T_{NI}), while the data for non-oriented samples are shown to the right.

ter and the nematic LCE network, along with the consequent reduction in mechanical properties, is an intrinsic characteristic of side-chain nematic LCEs, irrespective of the specific mesogen chemistry.

To further verify the growing role of swelling in the reduction of mechanical properties in non-oriented LCEs, we conduct MD simulations to examine the swelling behavior and mechanical response of C3M-based LCEs across a range of temperatures (Fig. 8). The simulation results align well with experimental findings, showing that mechanical strength decreases with increasing temperature, consistent with greater water uptake. Taken together, these experimental and computational results demonstrate that in non-oriented LCEs, reduction in mechanical properties arises predominantly from swelling effects, whereas in oriented LCEs, irreversible internal damage linked to disrupted mesogen alignment plays a larger role. This comparative insight highlights how molecular order fundamentally shapes the mechanisms of reduction in the mechanical properties of LCEs under aquatic and thermal conditions, providing a foundation for the rational design of more water-tolerant soft actuators.

5. Controlling water-induced reduction of mechanical properties in LCEs

Our results demonstrate that both oriented and non-oriented LCEs suffer a significant reduction in mechanical properties when exposed to water, driven by a combination of swelling and irreversible internal damage. This vulnerability fundamentally limits the reliable use of LCEs in underwater and humid environments, where consistent mechanical performance is critical for actuation, load-bearing, and long-term

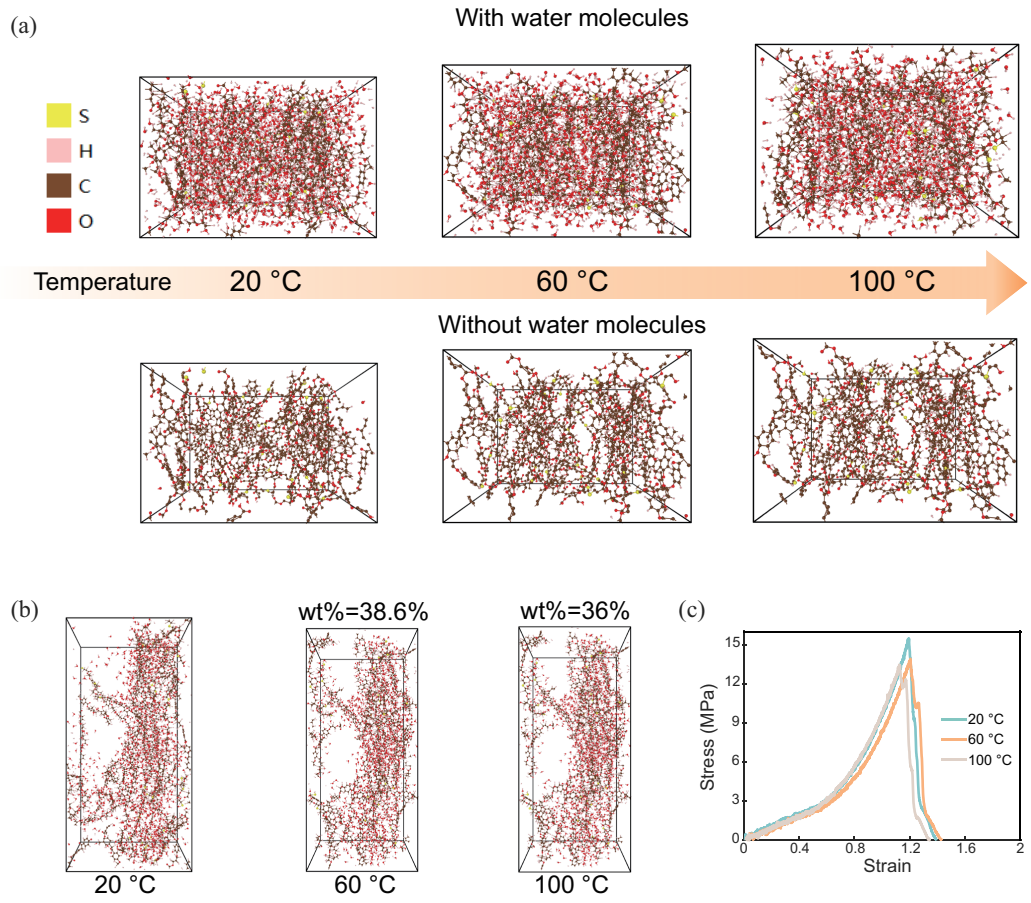

Figure 8 MD simulations of C3M-based LCEs under different soaking temperatures. (a) Molecular configurations of soaked LCE with/without water molecules under different soaking temperatures. (b) 3D representations of soaked LCEs under different soaking temperatures. (c) Stress-strain curves of LCEs after water soaking at different temperatures.

functionality.

Given that swelling and internal damage have been identified as primary mechanisms, we next explore strategies to systematically modulate these factors. Specifically, we investigate how controlling the extent of water absorption and mitigating network-level damage can improve the mechanical resilience of LCEs in water, thereby enhancing their potential for practical soft robotics and biomedical applications.

To address this challenge, we first focus on adjusting the material composition of LCEs to regulate swelling and internal damage. Specifically, we tune the oxygen content of C6M-based LCEs and the crosslink density of C3M-based LCEs to systematically investigate their effects on underwater mechanical stability. The oxygen content is varied by adjusting the amount of PEGDA, a high-oxygen-content component in the C6M-based LCE formulation, setting the molar ratio of liquid crystalline monomer C6M to PEGDA to 5/1, 7/1, and 9/1. The crosslink density is tuned by changing the molar ratio of PETMP to EDDET in the C3M-based LCE formulation; since PETMP introduces tetrafunctional crosslinking points, a higher proportion of PETMP results in a higher crosslink density. Accordingly, we set the EDDET to PETMP molar ratios to 9/1, 11/1, and 13/1.

To systematically evaluate how these compositional modifications affect water-induced swelling and mechanical degradation, all LCE samples with different oxygen contents and crosslink densities are soaked in water at room temperature for 24 h, followed by weighing to assess water uptake. A subset of the samples is then dehydrated. Both the soaked and dehydrated LCE samples are subjected to quasi-static tensile tests to evaluate their mechanical properties under different hydration states.

Based on these tests, experimental results show that LCEs with higher oxygen content exhibit greater water absorption (Fig. 9(a)), which leads to more pronounced decreases in tensile strength and elastic modulus after soaking (Fig. 9(b) and (c)). These LCEs with higher oxygen content also show improved recovery of mechanical properties upon dehydration, suggesting a relatively larger contribution of reversible swelling in the overall degradation process. This behavior may be attributed to the increased hydrophilicity and chain segment mobility introduced by oxygen-containing

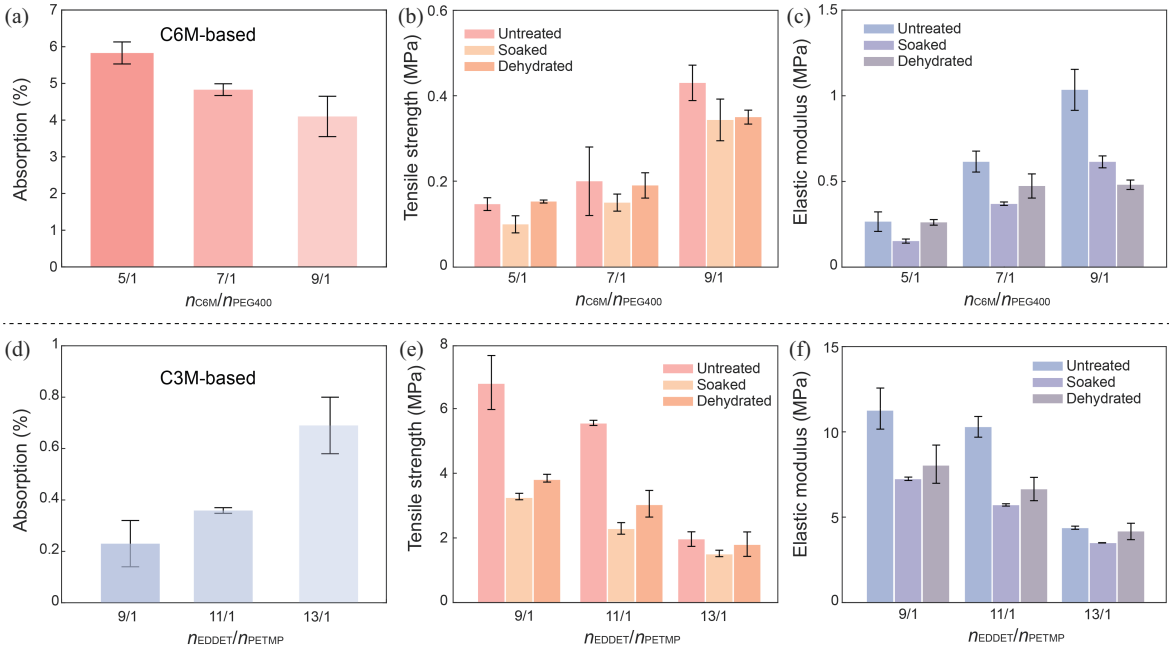

Figure 9 Mechanical properties of LCEs with different oxygen contents and crosslink densities when soaked in water. (a) Water absorption of C6M-based LCEs with different oxygen content. (b) Tensile strength and (c) elastic modulus of soaked/dehydrated C6M-based LCEs with different oxygen content. (d) Water absorption of C3M-based LCEs with different crosslink density. (e) Tensile strength and (f) elastic modulus of soaked/dehydrated C3M-based LCEs with different crosslink density.

groups, which facilitate network relaxation and partial self-reorganization during dehydration.

In parallel, for LCEs with varying crosslink density, those with lower crosslink density exhibit lower initial tensile strength and elastic modulus as well as higher water absorption, consistent with their more loosely connected network structure (Fig. 9(d)). Meanwhile, LCEs with lower crosslink density also show a greater recovery in mechanical performance after dehydration (Fig. 9(e) and (f)). We hypothesize that this behavior arises because a lowly crosslinked network is more flexible and more capable of accommodating volume expansion during soaking, leading to lower internal stress and thus less internal damage. Therefore, the lowly crosslinked network likely improves the mobility and relaxation of polymer chains during dehydration, helping the reorganization of the damaged structure.

While tuning oxygen content and crosslink density helps reduce internal damage, the reduction of mechanical properties due to swelling remains unavoidable. To further decouple and better understand the specific contribution of swelling to mechanical performance loss, we soak LCE samples in two additional liquids: absolute ethanol, which induces more severe swelling and potential damage than water, and silicone oil, which causes swelling without damaging the internal network. By comparing the mechanical behavior of LCEs after soaking in these three different liquids, we aim to gain deeper insight into the role of swelling in driving the reduction of mechanical properties (Fig. 10(a)–(c)).

We soak LCE samples in water and ethanol at room temperature for 24 h. For silicone oil, samples are soaked until reaching swelling saturation. After soaking, we conduct quasi-static tensile tests on both wet and dehydrated samples to evaluate changes in mechanical properties.

The experimental findings show that for the same soaking duration, ethanol induces significantly higher swelling and causes a more pronounced reduction in mechanical strength than both water and silicone oil (Fig. 10(d)–(i)). Although ethanol-swollen samples experience greater deformation, they exhibit better recovery of mechanical performance after dehydration compared to water-swollen samples, indicating that ethanol leads to less irreversible internal damage. In contrast, silicone oil causes no detectable internal damage, yet the LCEs still show a clear weakening of mechanical properties in the swollen state, which fully recovers upon drying. This contrast highlights that swelling alone, even without causing internal damage, can markedly deteriorate the mechanical properties of LCEs.

Therefore, to ensure robust mechanical behavior of LCEs under water-soaking, it is not sufficient to merely prevent irreversible internal damage; it is also essential to suppress the swelling behavior itself. To address this, we prepared a series of waterproof formulations by reducing the hydrophilic content in the LCE network either through replacing oxygen-containing crosslinkers with oxygen-free ones or even by

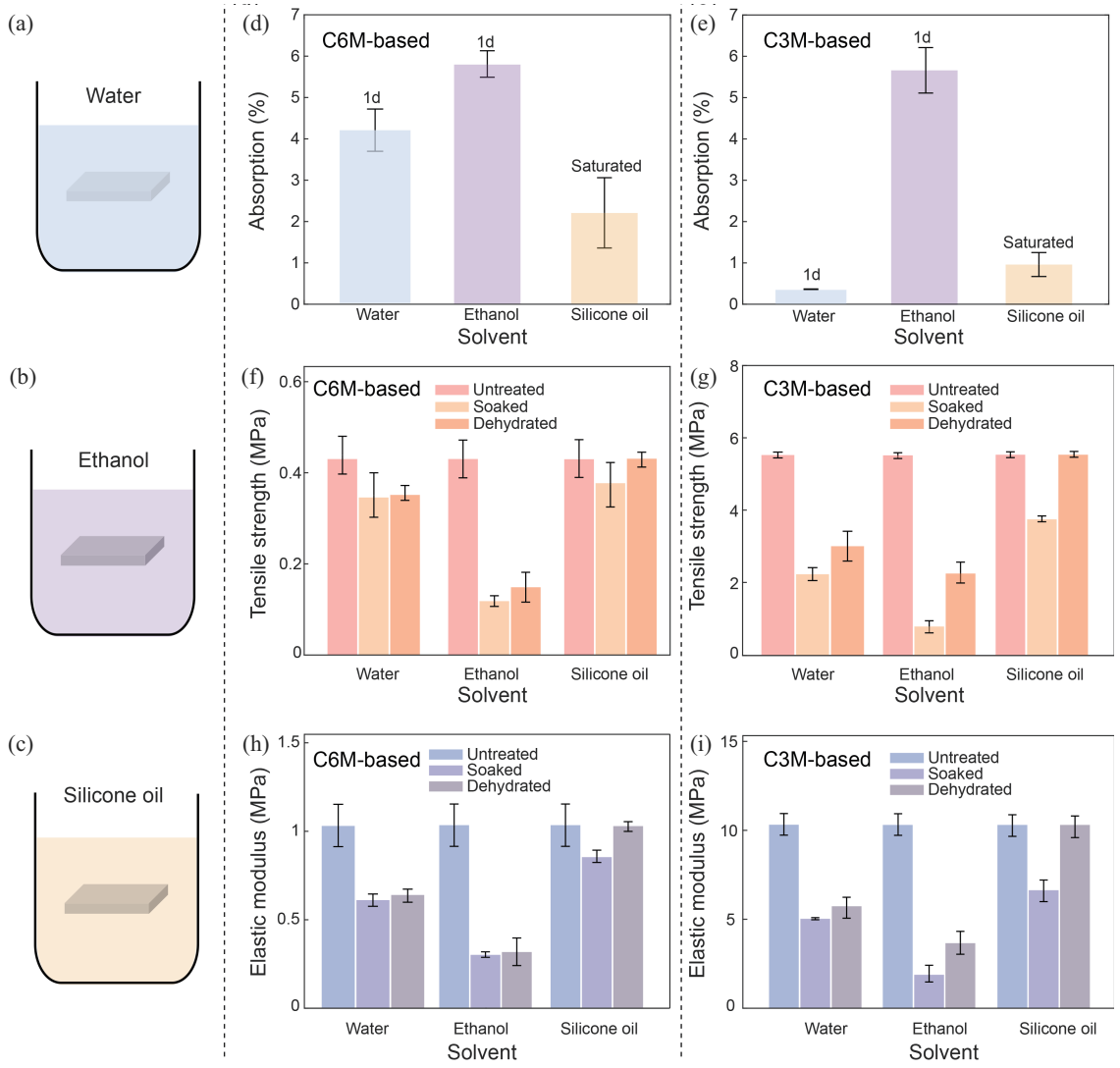

Figure 10 Mechanical properties of LCEs in different liquid environments. Schematic of LCEs soaked in (a) water, (b) ethanol, and (c) silicone oil. The absorption of (d) C6M-based LCEs and (e) C3M-based LCEs soaked in different liquid environments. The tensile strength of (f) C6M-based LCEs and (g) C3M-based LCEs when interacting with different liquid environments. The elastic modulus of (h) C6M-based LCEs and (i) C3M-based LCEs when interacting with different liquid environments.

eliminating crosslinkers entirely (Table 1). These modified LCEs were immersed in water for one week to assess their resistance to hydro-induced degradation. Despite the reduced hydrophilic content, all formulations still exhibited a decrease in mechanical performance, with a measurable reduction rate (defined as the ratio of the performance loss to the initial value) (Fig. 11). Although most samples recovered nearly all of their mechanical strength after dehydration, the results clearly demonstrate that even with water-resistant formulations, the degradation of mechanical properties under prolonged water exposure cannot be fully avoided.

To address this challenge, we apply a waterproof coating of butyl rubber with a molecular weight of 10000 on the surface of LCE samples and soak them in water for one week. After soaking, the coated LCEs show no whitening, indicating effective prevention of water absorption. Subsequent mechanical tests further confirm that their mechanical properties remain unchanged, and the thermal actuation performance is also unaffected (Fig. 12). Moreover, in Ref. [22], a similar butyl rubber coating was demonstrated to maintain, and even slightly enhance, the underwater actuation performance of LCEs by reducing heat dissipation to the surrounding water. These results demonstrate that, to ensure long-term underwater performance of LCEs, the most reliable approach

Table 1 Attempts of waterproof LCE formulations

Characteristics	Formula	Index
Without spacer	C6M + n-butylamine	1
Anaerobic spacer	C3M + propane-1,3-dithiol	2
Anaerobic spacer	C3M + 1,4-butanedithiol	3

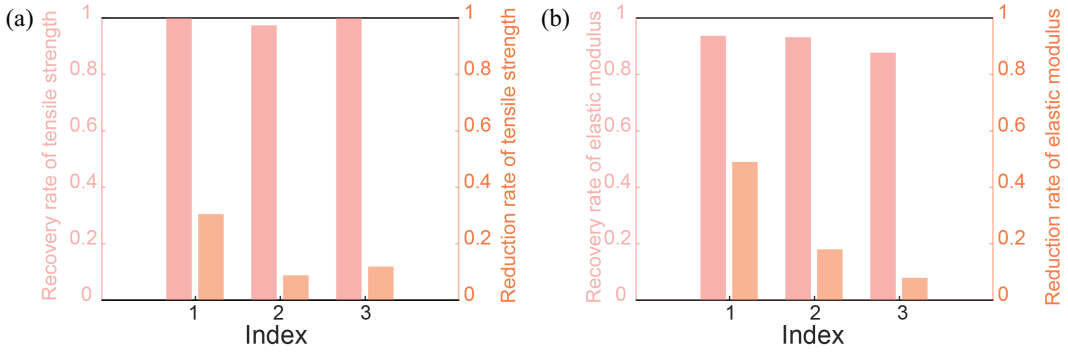

Figure 11 Recovery rate and reduction rate in mechanical properties of LCEs after 7 days with water-soaking and dehydration. (a) Recovery rate and reduction rate of tensile strength of LCEs with a waterproof formula. (b) Recovery rate and reduction rate of elastic modulus of LCEs with a waterproof formula. Both recovery rate and reduction rate are averaged over three samples.

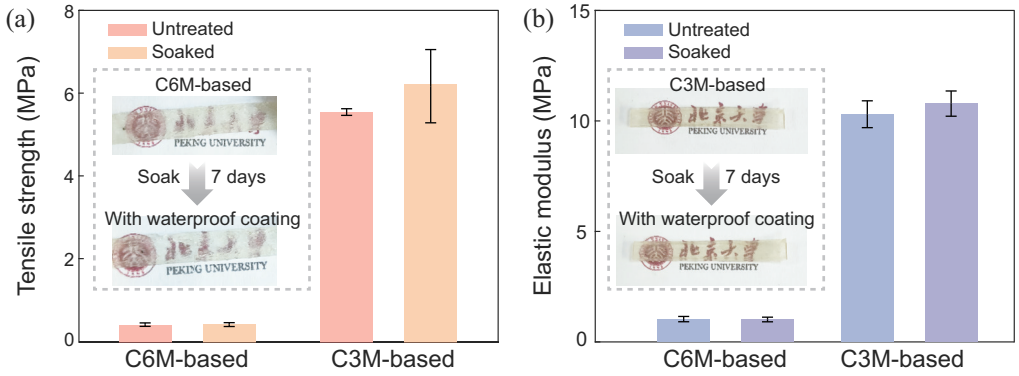

Figure 12 Mechanical properties of LCEs coated by uncured butyl rubber after 7 days of water-soaking. (a) Tensile strength of waterproof LCEs before and after soaking. The insets are the photographs of C6M-based LCEs before and after soaking. (b) Elastic modulus of waterproof LCEs before and after soaking. The insets are the photographs of C3M-based LCEs before and after soaking.

is to use an effective waterproof coating that physically blocks water penetration, thereby eliminating both swelling and water-induced damage. It is worth noting that the use of butyl rubber coatings, while highly effective in our study, may face potential challenges of delamination in practical applications. However, the selected butyl rubber formulation remains in a highly viscous, gel-like state that provides strong tackiness and conformal adhesion to the LCE substrate. No delamination was observed throughout our one-week soaking and testing process, indicating robust interfacial stability under the conditions examined. This highlights the critical role of surface protection strategies in achieving durable LCE-based soft actuators and devices.

6. Conclusions

In this work, we systematically investigate the effect of water on the mechanical properties of LCEs, focusing on materials based on two widely used liquid crystal monomers, C6M and C3M. Mechanical testing after swelling and drying shows that water negatively affects both oriented and non-oriented LCEs, with a more pronounced impact on the non-oriented ones. Combined MD and FTIR confirm that this deterioration results from both swelling and internal damage, with the latter playing a dominant role. By tuning the oxygen content and crosslink density of LCEs, we successfully reduce the extent of internal damage. However, tests in other solvents confirm that swelling alone reduces underwater mechanical properties even without internal damage. Further efforts to decrease hydrophilic functional groups at the network level show that it is still challenging to completely suppress water permeation and swelling, even when oxygen-containing crosslinkers are fully removed. Therefore, we propose the use of a waterproof coating as an effective physical barrier to block water ingress, representing the most practical and reliable strategy to achieve stable underwater mechanical performance of LCEs.

This study not only reveals the mechanism by which water affects LCEs' mechanical properties but also provides a comprehensive solution from material design to surface engineering. The findings offer fundamental insights and design guidelines for developing intelligent actuating materials and soft robots capable of long-term operation under water-soaking, thereby expanding the application potential of LCEs

in complex conditions.

Appendix A. Thermal analysis of LCEs

The DSC measurements were conducted using a Discovery DSC250 instrument (TA Instruments) under a nitrogen atmosphere. The heating and cooling processes were performed at a scanning rate of 40 °C/min, spanning a temperature range from –20 to 200 °C (Fig. A1). The T_{NI} of the LCEs were determined from the heating curves. Specifically, the C6M-based LCE exhibited a T_{NI} of 42.5 °C, while the C3M-based LCE showed a higher T_{NI} of 70.4 °C (Fig. A1).

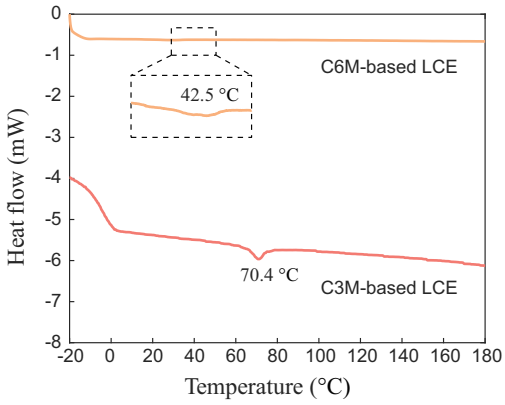

Figure A1 Thermal performance of LCEs. DSC heating curves of C6M-based and C3M-based LCEs.

Appendix B. Details of MD simulations

To investigate the microscopic mechanisms behind the water-induced volume change and mechanical response of LCEs, we conducted MD simulations. As shown in Fig. B1(a), the simulated swelling behavior of LCEs exhibits a clear increase in volume with increasing water absorption. This trend is consistent with experimental observations and reflects the disruption of physical crosslinks and the increase in free volume caused by water molecules penetrating the polymer network. The inset highlights the swelling ratio at different water absorption levels under various temperatures (20–100 °C), further confirming that higher temperatures promote water uptake and swelling.

In tensile simulations, LCEs show significantly higher tensile strength and elastic modulus compared to experimental results. This discrepancy primarily arises from the much higher strain rate employed in MD simulations due to the inherent limitations in simulation time scales. To validate this explanation, we conduct tensile tests at different stretching speeds (Fig. B1(b)). The results clearly indicate that both the tensile strength and elastic modulus increase with increasing stretch speed. Therefore, for consistency and reliability in our experiments, we chose a relatively stable and slow stretching speed of 10 mm/min, which better represents quasi-static conditions and minimizes dynamic effects.

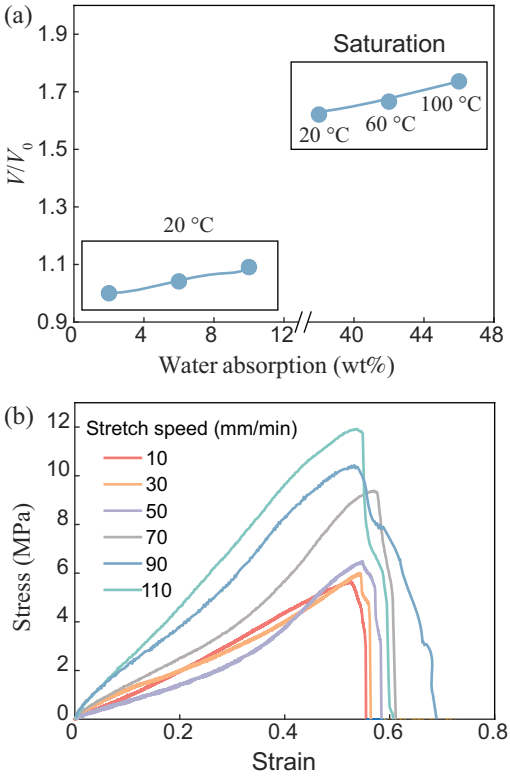

Figure B1 Details of MD simulations on LCEs. (a) Swelling behavior of LCEs obtained from MD simulations. (b) Tensile stress-strain curves of LCEs at different stretch speeds.

Appendix C. Fracture energy

To quantitatively evaluate the influence of water soaking on the mechanical integrity of the LCEs, we measured their fracture energy (Γ) using the pure shear test method [53, 54]. In this method, two rectangular samples (height = 5 mm, width = 50 mm, and thickness = 1 mm) were glued onto acrylic plates, and an edge notch (~10 mm) was introduced into one of them using a sharp razor blade. The notched sample was stretched monotonically until rupture, and the critical stretch (λ_c) was recorded. A pristine sample was also tested under identical conditions to obtain the stress-stretch curve for calculating the strain energy density $W(\lambda_c)$ between $\lambda = 1$ and $\lambda = \lambda_c$. The fracture energy was then determined as

$$\Gamma = W(\lambda_c)H,$$

where H is the undeformed sample height. All tests were performed at room temperature (20 °C) and a strain rate of 0.005 s^{-1}.

Both the C6M-based and C3M-based LCEs were immersed in water for 7 days and then dehydrated before testing. As shown in Fig. C1, water soaking led to a pronounced

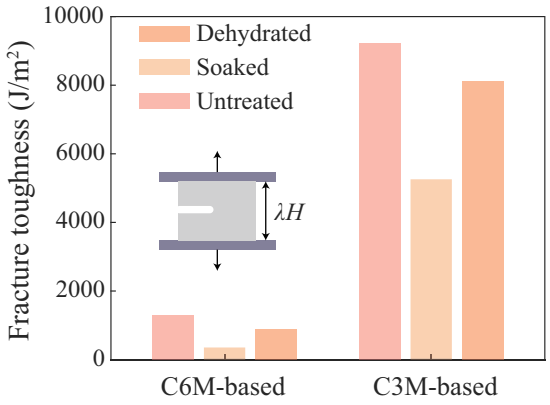

Figure C1 Fracture toughness (Γ) of C6M-based and C3M-based LCEs in untreated, soaked, and dehydrated states. The inset schematically illustrates the pure shear test configuration, where λH denotes the deformed height under tension.

decrease in fracture energy—by approximately 60% for the C6M-based and 37% for the C3M-based LCEs—indicating substantial deterioration in network toughness. Moreover, the fracture energy did not fully recover after dehydration, implying that the degradation arises not only from reversible swelling effects but also from irreversible chemical or microstructural damage to the polymer network.

Conflict of interest *On behalf of all authors, the corresponding author states that there is no conflict of interest.*

Author contributions ***Wenhui Chen:*** *Methodology, Software, Data curation, Investigation, Visualization, Writing – original draft, Writing – review & editing.* ***Xiaohang Zhou:*** *Methodology, Data curation, Writing – review & editing.* ***Junmou Tang:*** *Methodology.* ***Ruobing Bai:*** *Writing – review & editing.* ***Liu Wang:*** *Writing – review & editing.* ***Ke Liu:*** *Conceptualization, Project administration, Supervision, Writing – review & editing.*

Acknowledgements *This work was supported by the National Key Research and Development Program of China (Grant No. 2022YFB4701900), the Fundamental Research Funds for the Central Universities, Peking University, and the Opening Fund of State Key Laboratory of Nonlinear Mechanics.*

References

1 A. Kotikian, J. M. Morales, A. Lu, J. Mueller, Z. S. Davidson, J. W. Boley, and J. A. Lewis, Innervated, self-sensing liquid crystal elastomer actuators with closed loop control, Adv. Mater. **33**, 2101814 (2021).
2 S. Wu, Y. Hong, Y. Zhao, J. Yin, and Y. Zhu, Caterpillar-inspired soft crawling robot with distributed programmable thermal actuation, Sci. Adv. **9**, eadf8014 (2023).
3 J. Wu, S. Yao, H. Zhang, W. Man, Z. Bai, F. Zhang, X. Wang, D. Fang, and Y. Zhang, Liquid crystal elastomer metamaterials with giant biaxial thermal shrinkage for enhancing skin regeneration, Adv. Mater. **33**, 2106175 (2021).
4 K. Liu, F. Hacker, and C. Daraio, Robotic surfaces with reversible, spatiotemporal control for shape morphing and object manipulation, Sci. Robot. **6**, eabf5116 (2021).
5 W. Li, and X. S. Zhang, Arbitrary curvature programming of thermoactive liquid crystal elastomer via topology optimization, Comput. Meth. Appl. Mech. Eng. **417**, 116393 (2023).
6 M. Barnes, F. Feng, and J. S. Biggins, Surface instability in a nematic elastomer, Phys. Rev. Lett. **131**, 238101 (2023).
7 B. Chen, C. Liu, Z. Xu, Z. Wang, and R. Xiao, Modeling the thermo-responsive behaviors of polydomain and monodomain nematic liquid crystal elastomers, Mech. Mater. **188**, 104838 (2024).
8 W. Chen, R. Wang, and K. Liu, Active compliant mechanisms for optimized actuation by LCE-based artificial muscles, Mech. Mater. **189**, 104879 (2024).
9 R. Bai, and K. Bhattacharya, Photomechanical coupling in photoactive nematic elastomers, J. Mech. Phys. Solids **144**, 104115 (2020).
10 Z. Liu, H. K. Bisoyi, Y. Huang, M. Wang, H. Yang, and Q. Li, Thermo- and mechanochromic camouflage and self-healing in biomimetic soft actuators based on liquid crystal elastomers, Angew. Chem. Int. Ed. **61**, e202115755 (2022).
11 A. Kotikian, R. L. Truby, J. W. Boley, T. J. White, and J. A. Lewis, 3D printing of liquid crystal elastomeric actuators with spatially programed nematic order, Adv. Mater. **30**, 1706164 (2018).
12 A. Kotikian, C. McMahan, E. C. Davidson, J. M. Muhammad, R. D. Weeks, C. Daraio, and J. A. Lewis, Untethered soft robotic matter with passive control of shape morphing and propulsion, Sci. Robot. **4**, eaax7044 (2019).
13 R. S. Kularatne, H. Kim, J. M. Boothby, and T. H. Ware, Liquid crystal elastomer actuators: Synthesis, alignment, and applications, J. Polym. Sci. Pol. Phys. **55**, 395 (2017).
14 J. Chen, J. Jiang, J. Weber, V. Gimenez-Pinto, and C. Peng, Shape morphing by topological patterns and profiles in laser-cut liquid crystal elastomer Kirigami, ACS Appl. Mater. Interfaces **15**, 4538 (2023).
15 G. Wang, Z. Lei, J. Jiang, C. Peng, and C. Li, Complementing photothermal to photochemical actuation of assembled liquid crystal networks for wavelength-selective multimodal locomotion, Chem. Eng. J. **498**, 155254 (2024).
16 Z. Wei, U. H. Bootwala, and R. Bai, Synthesis-processing-property relationships in thermomechanics of liquid crystal elastomers, J. Mech. Phys. Solids **196**, 105977 (2025).
17 A. Das, J. M. McCracken, M. H. Saeed, D. Nepal, and T. J. White, Photodriven aquatic locomotion in liquid crystalline elastomer composites with tunable wettability, Angew. Chem. Int. Ed. **64**, e202505300 (2025).
18 M. Li, F. Gholami, L. Yue, M. R. Fratarcangeli, E. Black, S. Shimokawa, T. Nomura, M. Tanaka, H. Kobayashi, Y. Song, and H. J. Qi, Coaxial-spun hollow liquid crystal elastomer fiber as a versatile platform for functional composites, Adv. Funct. Mater. **34**, 2406847 (2024).
19 J. Jiang, Y. Ma, R. Cheng, and Y. Zhao, A porous multi-stimuli-responsive liquid crystal elastomer actuator enabled by Mof loading, Adv. Funct. Mater. **34**, 2313625 (2024).
20 Q. Chen, J. Huang, X. Feng, H. Xie, and S. Zhou, Controlling self-oscillation of a single-layer liquid crystal elastomer at the air-water interface via light programming for water strider-inspired aquatic robots, ACS Appl. Mater. Interfaces **17**, 17433 (2025).
21 M. Barnes, and J. S. Biggins, Microstructural basis of complex mechanical programming in liquid crystal elastomers, J. Elast. **157**, 48 (2025).
22 W. Chen, S. Yang, C. Zhu, Y. Cheng, Y. Shi, C. Yu, and K. Liu, Scalable jet swimmer driven by pulsatile artificial muscles and soft chamber buckling, Adv. Mater. **37**, 2503777 (2025).
23 W. Chen, D. Tong, L. Meng, B. Tan, R. Lan, Q. Zhang, H. Yang, C. Wang, and K. Liu, Knotted artificial muscles for bio-mimetic actuation under deepwater, Adv. Mater. **36**, 2400763 (2024).
24 K. Kim, Y. Guo, J. Bae, S. Choi, H. Y. Song, S. Park, K. Hyun, and S. Ahn, 4D printing of hygroscopic liquid crystal elastomer actuators, Small **17**, 2100910 (2021).
25 Q. He, Z. Wang, Y. Wang, Z. Song, and S. Cai, Recyclable and self-repairable fluid-driven liquid crystal elastomer actuator, ACS Appl. Mater. Interfaces **12**, 35464 (2020).
26 L. Xu, S. Zhang, L. Yin, and Y. Zhao, Humidity-sensing and moisture-steering liquid crystal elastomer actuator, Small **21**, 2412547 (2025).

27 A. Rey, and R. Zmeureanu, Multi-objective optimization framework for the selection of configuration and equipment sizing of solar thermal combisystems, Energy **145**, 182 (2018).
28 V. Maurin, Y. Chang, Q. Ze, S. Leanza, J. Wang, and R. R. Zhao, Liquid crystal elastomer-liquid metal composite: Ultrafast, untethered, and programmable actuation by induction heating, Adv. Mater. **36**, 2302765 (2024).
29 G. Babakhanova, H. Yu, I. Chaganava, Q. H. Wei, P. Shiller, and O. D. Lavrentovich, Controlled placement of microparticles at the water-liquid crystal elastomer interface, ACS Appl. Mater. Interfaces **11**, 15007 (2019).
30 R. Liang, H. Yu, L. Wang, and D. Shen, Light-guided dynamic liquid crystalline elastomer actuators enabled by mussel adhesive protein chemistry, Adv. Funct. Mater. **33**, 2211914 (2023).
31 W. Liao, and Z. Yang, 3D printing programmable liquid crystal elastomer soft pneumatic actuators, Mater. Horiz. **10**, 576 (2023).
32 Y. Cui, Y. Yin, C. Wang, K. Sim, Y. Li, C. Yu, and J. Song, Transient thermo-mechanical analysis for bimorph soft robot based on thermally responsive liquid crystal elastomers, Appl. Math. Mech.-Engl. Ed. **40**, 943 (2019).
33 T. Zhao, J. Wang, Y. Fan, and W. Dou, Helical liquid crystal elastomer miniature robot with photocontrolled locomotion, Adv. Mater. Technol. **7**, 2200222 (2022).
34 N. P. Pinchin, H. Guo, H. Meteling, Z. Deng, A. Priimagi, and H. Shahsavan, Liquid crystal networks meet water: It's complicated! Adv. Mater. **36**, 2303740 (2024).
35 C. Zhao, Z. Chen, R. Shi, X. Yang, and T. Zhang, Recent advances in conjugated polymers for visible-light-driven water splitting, Adv. Mater. **32**, 1907296 (2020).
36 M. A. Azka, S. M. Sapuan, H. Abral, E. S. Zainudin, and F. A. Aziz, An examination of recent research of water absorption behavior of natural fiber reinforced polylactic acid (PLA) composites: A review, Int. J. Biol. Macromol. **268**, 131845 (2024).
37 Z. Zhang, H. Fu, Z. Li, J. Huang, Z. Xu, Y. Lai, X. Qian, and S. Zhang, Hydrogel materials for sustainable water resources harvesting & treatment: Synthesis, mechanism and applications, Chem. Eng. J. **439**, 135756 (2022).
38 L. N. Woodard, and M. A. Grunlan, Hydrolytic degradation and erosion of polyester biomaterials, ACS Macro Lett. **7**, 976 (2018).
39 P. C. F. Buchholz, G. Feuerriegel, H. Zhang, P. Perez-Garcia, L. L. Nover, J. Chow, W. R. Streit, and J. Pleiss, Plastics degradation by hydrolytic enzymes: The plastics-active enzymes database—PAZy, Proteins **90**, 1443 (2022).
40 C. Medina Jaramillo, T. J. Gutiérrez, S. Goyanes, C. Bernal, and L. Famá, Biodegradability and plasticizing effect of yerba mate extract on cassava starch edible films, Carbohyd. Polym. **151**, 150 (2016).
41 E. Basiak, A. Lenart, and F. Debeaufort, How glycerol and water contents affect the structural and functional properties of starch-based edible films, Polymers **10**, 412 (2018).
42 B. Song, D. Landry, T. Martinez, C. N. Chung, K. N. Long, K. Yu, and C. M. Yakacki, On the effect of strain rate during the cyclic compressive loading of liquid crystal elastomers and their 3D printed lattices, Mech. Mater. **197**, 105086 (2024).
43 Z. Siddiqui, J. Smay, and A. Azoug, Highly tunable actuation and mechanical properties of 4D-printed nematic liquid crystal elastomers, Mech. Mater. **170**, 104329 (2022).
44 C. Wang, K. Sim, J. Chen, H. Kim, Z. Rao, Y. Li, W. Chen, J. Song, R. Verduzco, and C. Yu, Soft ultrathin electronics innervated adaptive fully soft robots, Adv. Mater. **30**, 1706695 (2018).
45 J. Liu, X. Zhu, Z. Shen, and Y. Zhang, Imperfection sensitivity of mechanical properties in soft network materials with horseshoe microstructures, Acta Mech. Sin. **37**, 1050 (2021).
46 L. Martínez, R. Andrade, E. G. Birgin, and J. M. Martínez, PACKMOL: A package for building initial configurations for molecular dynamics simulations, J. Comput. Chem. **30**, 2157 (2009).
47 S. Plimpton, Fast parallel algorithms for short-range molecular dynamics, J. Comput. Phys. **117**, 1 (1995).
48 W. L. Jorgensen, and J. Tirado-Rives, The OPLS potential functions for proteins, energy minimizations for crystals of cyclic peptides and crambin, J. Am. Chem. Soc. **110**, 1657 (1988).
49 W. L. Jorgensen, J. Chandrasekhar, J. D. Madura, R. W. Impey, and M. L. Klein, Comparison of simple potential functions for simulating liquid water, J. Chem. Phys. **79**, 926 (1983).
50 S. Schott-Verdugo, and H. Gohlke, PACKMOL-Memgen: A simple-to-use, generalized workflow for membrane-protein-lipid-bilayer system building, J. Chem. Inf. Model. **59**, 2522 (2019).
51 N. Nayir, A. C. T. van Duin, and S. Erkoc, Development of a ReaxFF reactive force field for interstitial oxygen in germanium and its application to GeO_2/Ge interfaces, J. Phys. Chem. C **123**, 1208 (2019).
52 W. Gonçalves, T. Mabuchi, and T. Tokumasu, Nucleation and growth of cavities in hydrated Nafion membranes under tensile strain: A molecular dynamics study, J. Phys. Chem. C **123**, 28958 (2019).
53 R. Annapooranan, Y. Wang, and S. Cai, Highly durable and tough liquid crystal elastomers, ACS Appl. Mater. Interfaces **14**, 2006 (2022).
54 R. S. Rivlin, and A. G. Thomas, Rupture of rubber. I. Characteristic energy for tearing, J. Polym. Sci. **10**, 291 (1953).

水浸作用对液晶弹性体力学性能影响的实验研究

陈雯慧, 周晓航, 唐君谋, 白若冰, 王柳, 刘珂

摘要 液晶弹性体(LCEs)作为驱动软体机器人的人造肌肉应用日益广泛. 尽管其在空气与水中的驱动形变相似, 但实验表明, 水浸泡会显著导致LCEs力学性能下降, 制约了其水下长期应用. 本研究以两种常用液晶单体(C6M与C3M)为对象, 系统揭示了水影响LCEs力学性能的机理. 通过浸泡-脱水实验、力学测试、分子动力学模拟及傅里叶变换红外光谱分析, 我们发现水分会同时引发材料溶胀与化学降解, 从而显著降低其机械强度. 尽管尝试了调控氧含量、改变交联密度、剔除含氧交联剂等多种策略, 但因无法根本解决溶胀与降解问题, 效果均有限. 最终, 我们提出并验证了一种有效的防水策略—采用丁基橡胶液体涂层进行封装. 本研究为理解水环境下LCEs的力学行为提供了理论依据, 也为开发耐久的水下LCE软体机器人提供了实用指导.